Miscibilization of Reactive Polymers during Early-Stage Spinodal Decomposition

Victor V. Yashin and Richard J. Spontak
Depts. of Materials Science and Engineering and Chemical Engineering, North Carolina State University, Raleigh, NC 27695

Reactive compatibilization constitutes an important method by which to control the size scale of phase separation in immiscible polymer blends. If a polymer pair exhibits a miscibility window at experimentally accessible temperatures, then reactive chain coupling can also be used to enhance the miscibility of the blend during spinodal decomposition in the biphasic region. We consider here the simultaneous phase separation and chemical reaction of A and B homopolymer blends in which end-functionalized A chains react with a variety of functionalized B chains to form either AB diblock, ABA triblock, or $\bar{n}$-armed B-g-A graft copolymers. Analytical expressions for the structure factors and Onsager kinetic coefficients are developed for each of these copolymer architectures in the kinetically controlled mean-field limit of early-stage spinodal decomposition. Multifunctional conversion-architecture-phase stability (CAPS) diagrams are introduced to facilitate comparison of the effect of copolymer architecture on reaction-driven blend miscibilization.

Introduction

Unlike their small-molecule analogs, macromolecules are generally immiscible due to their low entropy of mixing. Production of advanced polymer blends with properties tailored for commercial applications can consequently be frustrated, since the mechanical performance and stability of such blends are strongly dependent on interfacial adhesion (Wool, 1995). Attempts to improve the properties of blends composed of two highly incompatible homopolymers (designated A and B) rely extensively on the addition of a premade emulsifying agent, such as a block or graft copolymer. Linear block copolymers are composed of two or more long, contiguous monomer sequences ("blocks") that are covalently linked to form a backbone, whereas graft (or comb block) copolymers consist of a backbone of one monomer species and side grafts (arms) of another. Such copolymers are thermodynamically driven to the A/B interface, where they serve to reduce interfacial tension (and the size scale of phase separation), thereby enhancing phase intimacy (Noolandi and Hong, 1982; Bates, 1991; Piirma, 1992; Milner, 1997). Since they are used to achieve the same result as small-molecule surfactants in oil/water emulsions (namely, control over domain size), block and graft copolymers are commonly referred to as macromolecular surfactants.

The design of a compatibilized polymer blend begins with two homopolymers that possess properties relevant to a specific application but, because of their incompatibility, do not exhibit an accessible miscibility window. Control over the size and adhesion of phase-separated domains during copolymer-driven compatibilization requires consideration of several factors: (1) copolymer block length, to ensure effective copolymer–homopolymer entanglement (Creton et al., 1991; Cigana et al., 1996; Lyatskaya et al., 1995, 1996); (2) copolymer concentration, to avoid separation of the copolymer into its own phase (Dai et al., 1994, 1997); and (3) phase-separation kinetics, to promote copolymer diffusion to the A/B interface in a high-viscosity polymer melt (Hashimoto and Izumitani, 1993; Macosko et al., 1996). Another route by which to compatibilize immiscible homopolymers is through reactive blending, in which functionalized A and B chains are covalently or specifically coupled (through, e.g., ion complexation or hydrogen bonding) during melt processing (Bonner and Hope, 1993; Fleischer et al., 1994; Scott and Macosko, 1994, 1995; Guégan et al., 1994; Sundararaj and Macosko, 1995; Kumpf et al., 1995; Feng et al., 1996). Since such blending results in the *in situ* formation of block or graft copoly-

Correspondence concerning this article should be addressed to R. J. Spontak.
Present address of V. V. Yashin: Institute of Polymer Engineering, University of Akron, Akron, OH 44325.

mers, domain sizes are regulated through shear-induced mixing and chemical reaction. While experimental studies of reactive polymer blends can be performed to emulate commercial conditions, complementary theoretical efforts (Fredrickson and Milner, 1996; Fredrickson and Leibler, 1996; O'Shaughnessy and Sawhney, 1996) have to analyze this complex process without much reliance on related problems.

Commercial reactive compatibilization constitutes an example of a dynamic process in which interface formation is promoted. The general concept of reactive polymer blending can, however, be extended to a related process directed at enhancing the *miscibility* of phase-separating polymer blends that are intrinsically miscible over experimentally accessible temperature ranges (Balsara, 1996). In such a blend, functionalized chain coupling can serve to either enlarge the single-phase region of the phase diagram or alter the phase diagram altogether. Several temperature-sensitive association–dissociation macromolecular reactions have, for instance, been found to induce a lower critical solution temperature (LCST) in a polymer blend for which the parent (unfunctionalized) blend exhibits an upper critical solution temperature (UCST) (He et al., 1991; Feng et al., 1996). Since reactive blending in this context clearly differs from that commonly employed in commercial *compatibilization*, we refer to this process as reactive *miscibilization*, although we note that miscibilization constitutes a limiting case of compatibilization (Datta and Lohse, 1996).

To discern the relative importance of copolymer architecture on reactive miscibilization and blend dynamics, a theoretical formalism capable of distinguishing among various copolymer architectures, while addressing simultaneous macromolecular reactions and transport processes, is needed. Here, we consider the case of a polymer mixture composed of partially functionalized homopolymers prepared in such a way (through, e.g., freeze-drying or rapid solvent evaporation of single-phase polymer solutions) so that the resulting blend, in the absence of imposed flow, remains initially homogeneous in the unstable (two-phase) region of the phase diagram (He et al., 1991; Tanaka et al., 1992; Platé et al., 1995; Feng et al., 1996). In this case, phase separation in the blend is governed by reaction and interdiffusion of the constituent chains. Since *in situ* copolymer formation occurs relatively slowly (Guégan et al., 1994), the chain-coupling reaction can be considered kinetically controlled in slightly inhomogeneous blends, and the concurrent reaction-diffusion process can be described in terms of a mean-field treatment (de Gennes, 1982a, 1982b; O'Shaughnessy, 1994; Yashin et al., 1997). Such an analysis is clearly restricted to the onset of spinodal decomposition and the region of the blend phase diagram near the spinodal line. In the present work, we extend the use of the random phase approximation (de Gennes, 1979) to explore the roles of copolymer architecture, chain length, blend composition, and chemical incompatibility during reactive miscibilization of a polymer blend within this kinetically controlled regime.

Theoretical Framework

Molecular design of copolymer architectures

Consider a blend composed of two immiscible, monomolecular A and B homopolymers possessing degrees of polymerization N_A and N_B, respectively, and exhibiting UCST behavior. The number and placement of functionalized sites on the A and B chains are systematically varied so that these homopolymers react with each other to form one of three copolymer architectures:

AB Diblock Copolymers. The A and B chains are each functionalized at only one end.

ABA Triblock Copolymers. The A chains are functionalized at one end, while the B chains are functionalized at both ends.

B-g-A Graft Copolymers. The A chains are functionalized at one end, while sites along the B chains are functionalized.

These three coupling schemes are illustrated in Figure 1. The coupling reaction is assumed to be irreversible (consideration of polymer blends exhibiting LCST behavior is consequently beyond the scope of the present work). With monofunctionalized A chains, the copolymer molecular architecture depends on the number and location of reacting sites on the B chains. For the linear block copolymers, the number of sites (n) is either 1 (for the diblock) or 2 (for the triblock). In the case of B-*g*-A graft copolymers, the functionalized sites are presumed to be randomly placed along each B chain according to a Poisson distribution (with a mean value of $\bar{n}$). Since the A and B chains chemically combine to form copolymer molecules with N A+B repeat units, it is convenient here to introduce the copolymer composition as $f = N_A/N$. Note, however, that not all A and B chains are necessarily functionalized and participate in the coupling reaction, in

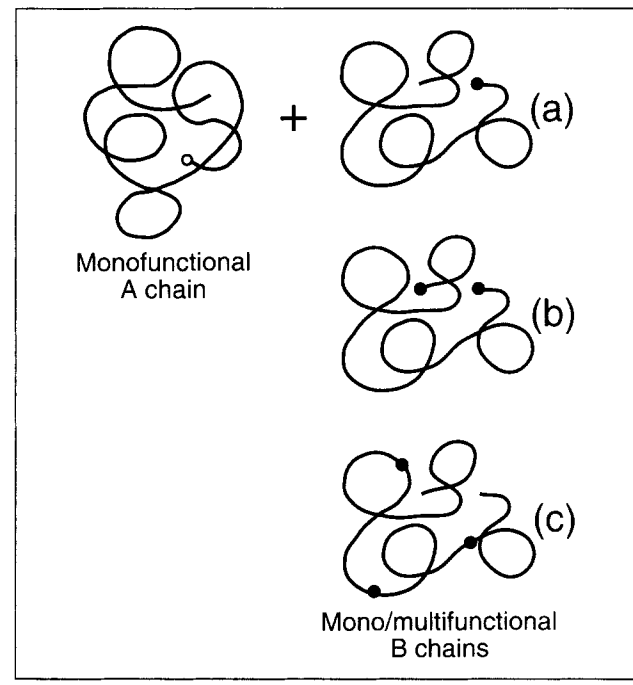

Figure 1. Coupling schemes considered in the present theoretical framework.

Each A chain possesses at most one functionalized endgroup. Every B chain can possess either one functionalized endgroup to form a coupled diblock (AB) copolymer (a), two functionalized endgroups to form a triblock (ABA) copolymer (b), or $\bar{n}$ functionalized sites along the chain to form a graft copolymer (B-*g*-A) with an average of $\bar{n}$ grafts or arms per copolymer molecule (c). Reactive sites are denoted by (○) and (●) on the A and B chains, respectively.

which case the concentrations of reactive sites a and b on the A and B chains are assigned z_a and z_b, respectively. Only in the event that $z_a = 1.00$ would all of the A homopolymer chains comprising the blend be capable of reacting to form copolymers. In addition, the volume-fraction composition of A in the blend is denoted by ϕ, while that of B is $1-\phi$.

Spinodal decomposition of nonreacting blends

The blend of A and B chains is prepared so that it is homogeneous in the glassy state (e.g., by freeze-drying a polymer–polymer–solvent solution) and so that its χ, the Flory–Huggins interaction parameter (which scales as reciprocal temperature), exceeds χ_c, the critical χ denoting the onset of phase instability (see Figure 2). If the blend is rapidly heated into the melt, it is expected to remain quasi-homogeneous (i.e., lacking interfacial structure) at time $t = 0$. During the subsequent course of spinodal decomposition, composition fluctuations grow and can be expressed in terms of the structure factor S, which reflects the time-dependent correlation of such fluctuations:

$$S(q,t) = \langle \delta\phi(\boldsymbol{q},t)\delta\phi(-\boldsymbol{q},t)\rangle, \tag{1}$$

where q corresponds to the magnitude of the wave vector $\boldsymbol{q}$, and the brackets indicate an averaging protocol. The linear (onset) stage of spinodal decomposition for a nonreacting blend is described by (Binder, 1994)

$$\frac{dS(q,t)}{dt} = -2q^2\Gamma(q)\Lambda S(q,t) + 2q^2\Lambda, \tag{2}$$

where $\Gamma(q)$ is the inverse equilibrium structure factor at a given temperature, and Λ is the Onsager interdiffusion kinetic coefficient. Within the random phase approximation (de Gennes, 1979), $\Gamma(q)$ is written as

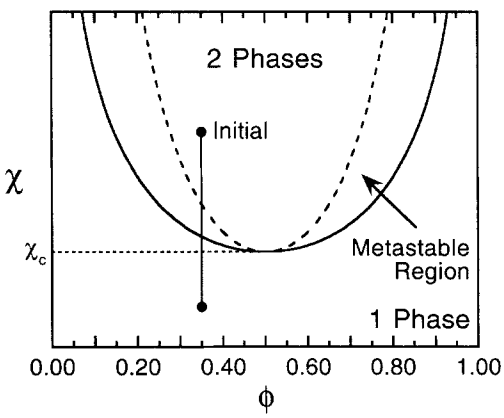

Figure 2. Idealized phase diagram, expressed in terms of χ ($\sim 1/T$) and ϕ, of a binary polymer blend exhibiting UCST (upper critical solution temperature) behavior.

Shown here are the binodal and spinodal curves (solid and dashed lines, respectively), as well as the unstable and two-phase regions. The theoretical framework proposed here requires an initial quench into the two-phase region so that $\chi > \chi_c$ (χ_c denotes the critical point where the binodal and spinodal curves converge).

$$\Gamma(q) = \frac{S_{aa}(q) + 2S_{ab}(q) + S_{bb}(q)}{S_{aa}(q)S_{bb}(q) - S_{ab}^2(q)} - 2\chi. \tag{3}$$

These S_{ij} ($i,j = a$ or b) denote the intrachain correlation functions for a system of noninteracting Gaussian chains. For linear homopolymers, the "bare" structure factors ($S_{ij}^{(0)}$) are given by (Binder, 1994)

$$S_{aa}^{(0)} = \phi N_A g_A \tag{4a}$$

$$S_{bb}^{(0)} = (1-\phi)N_B g_B \tag{4b}$$

$$S_{ab}^{(0)} = 0, \tag{4c}$$

where g_i (i = A or B) denotes the Debye scattering function $g_D(x_i)$, viz.,

$$g_D(x_i) = \frac{2}{x_i^2}(x_i + e^{x_i} - 1) \tag{5}$$

and

$$x_i = \frac{q^2a^2N_i}{6}. \tag{6}$$

Here, a corresponds to the size of a repeat unit. Note that only those fluctuations for which $\Gamma(q) < 0$ grow during spinodal decomposition.

In Eq. 2, the Onsager kinetic coefficient (Λ) depends on the diffusivities of the blend components. Generally speaking, Λ is a function of q at spatial scales on the order of a polymer coil size or less. Since this q-dependence is beyond the accuracy of the framework developed here, Λ is assumed to be independent of q. As a consequence, the explicit form of Λ can be determined from the fast-mode theory (Kramer et al., 1984; Sillescu, 1987; Kawasaki and Sekimoto, 1989), which yields the following for a binary blend of linear A and B homopolymers:

$$\Lambda = (1-\phi)^2\Lambda_A + \phi^2\Lambda_B, \tag{7}$$

where

$$\Lambda_A = \phi N_A D_A \tag{8a}$$

$$\Lambda_B = (1-\phi)N_B D_B. \tag{8b}$$

Here, D_i (i = A or B) is the self-diffusion coefficient of type-i polymer chain. If these linear chains are sufficiently long so that reptation (de Gennes, 1971) constitutes the principal mode of chain mobility, the A and B self-diffusion coefficients are proportional to N_A^{-2} and N_B^{-2}, respectively.

Spinodal decomposition of reacting blends

If the initially glassy blend is heated into the melt quickly enough to neglect the onset of chemical reaction during the course of heating, reactive chain coupling commences simultaneously with spinodal decomposition. In the event of concurrent spinodal decomposition and chemical reaction, both

Γ and Λ become time-dependent, since they are functions of blend composition, which varies with the extent of chain coupling. While the A and B units retain their chemical identity during the reaction (in which case Eq. 2 requires no additional terms), the architectures of at least some of the resident molecules change as copolymerization proceeds. Thus, the functional forms of S_{ij} and Λ differ from those provided in the last section addressing nonreacting blends. To account for this difference, we must first consider the extent of reaction conversion, p_i ($i = a$ or b), given by

$$p_i(t) = 1 - \frac{c_i(t)}{c_i(0)}, \tag{9}$$

where c_i is the time-dependent concentration of reactive sites on type-i chains. Analogous to the Debye scattering function in Eq. 5, the function h_i (i = A or B) is defined such that

$$h(x_i) = \frac{1 - e^{-x_i}}{x_i}. \tag{10}$$

The combination $\psi/(a^3N)$ is introduced to denote the average concentration of reacting sites on the B chains:

Diblock Copolymer Formation

$$\psi^{(2)} = \frac{z_b(1-\phi)}{1-f}. \tag{11}$$

Triblock Copolymer Formation

$$\psi^{(3)} = \frac{2z_b(1-\phi)}{1-f}. \tag{12}$$

Graft Copolymer Formation

$$\psi^{(g)} = \frac{\bar{n}z_b(1-\phi)}{1-f}. \tag{13}$$

Thus, ψ is a general parameter that effectively governs the process of miscibilization. By keeping ψ constant for all of the reaction types examined here, the relative miscibilization effectiveness of diblock (2), triblock (3), and graft (g) copolymers (measured in terms of the reaction time required to reach the spinodal condition) can be ascertained.

The structure factors S_{ij} derived for reacting blends of functionalized A and B homopolymers (and required in the calculation of Γ in Eq. 3) are provided below:

Diblock Copolymer Formation

$$S_{aa} = S_{aa}^{(0)} \tag{14a}$$

$$S_{bb} = S_{bb}^{(0)} \tag{14b}$$

$$S_{ab} = \psi^{(2)} N p_b f(1-f) h_A h_B. \tag{14c}$$

Triblock Copolymer Formation

$$S_{aa} = S_{aa}^{(0)} + \psi^{(3)} N f^2 p_b^2 h_A^2 e^{-x_B} \tag{15a}$$

$$S_{bb} = S_{bb}^{(0)} \tag{15b}$$

$$S_{ab} = \psi^{(3)} N p_b f(1-f) h_A h_B. \tag{15c}$$

Graft Copolymer Formation

$$S_{aa} = S_{aa}^{(0)} + \psi^{(g)} \bar{n} N f^2 p_b^2 h_A^2 g_B \tag{16a}$$

$$S_{bb} = S_{bb}^{(0)} \tag{16b}$$

$$S_{ab} = \psi^{(g)} N p_b f(1-f) h_A g_B. \tag{16c}$$

The Onsager kinetic coefficient (Λ) defined by Eqs. 7 and 8 corresponds to a binary blend of linear homopolymers and must be modified if new macromolecules are formed during the course of reactive chain coupling. It can be shown that, within the framework of the fast-mode theory (Kramer et al., 1984; Sillescu, 1987; Kawasaki and Sekimoto, 1989), the desired Onsager coefficients can be written as

Diblock Copolymer Formation

$$\Lambda = (1-\phi)^2(1 - z_a p_a)\Lambda_A + \phi^2(1 - z_b p_b)\Lambda_B + (\phi - f)^2 p_b \Lambda_D. \tag{17}$$

Triblock Copolymer Formation

$$\Lambda = (1-\phi)^2(1 - z_a p_a)\Lambda_A + \phi^2\left\{1 - z_b\left[1 - (1-p_b)^2\right]\right\}\Lambda_B + \left[\frac{p_b^2}{2}\left(\frac{\phi - f(2-\phi)}{1+f}\right)^2 + p_b(1-p_b)(\phi - f)^2\right]\Lambda_D. \tag{18}$$

Graft Copolymer Formation

$$\Lambda = (1-\phi)^2(1 - z_a p_a)\Lambda_A + \phi^2\{1 - z_b[1 - \exp(-\bar{n}p_b)]\}\Lambda_B. \tag{19}$$

The values of Λ_A and Λ_B are given by Eqs. 8a and 8b, respectively. Self-diffusion coefficients of linear macromolecules of length N are proportional to D, which scales as N^{-2} in the reptation regime. In this case, $D_i/D = N^2/N_i^2$ (i = A or B), and since $f = N_A/N$, it follows that

$$D_A = Df^{-2} \tag{20a}$$

$$D_B = D(1-f)^{-2}. \tag{20b}$$

In Eqs. 17 and 18, Λ_D is defined as $\psi^{(2)}ND$. The diffusivity of graft-copolymer chains is neglected in the derivation of Eq. 19 since such chains are effectively immobilized due to the presence of grafts.

It must be borne in mind that this framework is restricted to macromolecular reactions that are kinetically controlled. In this regime, mean-field approximations have been shown to be applicable (O'Shaughnessy, 1994), particularly when (1) a sufficiently large fraction of overlapping functionalized chains participate in the reaction, and (2) the blend is macroscopically homogeneous at the onset of spinodal decomposi-

tion. Within this regime, the reaction kinetics (required to discern the time dependence of the coefficients in Eq. 2) can be assumed to be of second order, in which case

$$\frac{dc_a}{dt} = -\alpha c_a c_b \tag{21a}$$

$$\frac{dc_b}{dt} = -\alpha c_a c_b. \tag{21b}$$

Here, α denotes the rate constant of the reaction. Solution of Eq. 21 yields the time-dependent reaction conversions p_i ($i = a$ or b), namely,

$$p_a(t) = \frac{c_b(0)}{c_a(0)} p_b(t) \tag{22a}$$

$$p_b(t) = \frac{1 - \exp\{-[c_b(0) - c_a(0)]\alpha t\}}{\frac{c_b(0)}{c_a(0)} - \exp\{-[c_b(0) - c_a(0)]\alpha t\}}, \tag{22b}$$

where the initial concentrations, $c_i(0)$, are given by

$$c_a(0) = \frac{z_a \phi}{a^3 f N} \tag{23a}$$

$$c_b(0) = \frac{\psi}{a^3 N}. \tag{23b}$$

From Eq. 2, it immediately follows that

$$S(q,t) = S(q,0)\exp\left[-2q^2\int_0^t \Lambda(\tau)\Gamma(q,\tau)\,d\tau\right] + 2q^2\int_0^t \Lambda(\tau)\exp\left[-2q^2\int_\tau^t \Lambda(\tau')\Gamma(q,\tau')\,d\tau'\right]d\tau, \tag{24}$$

where $\Gamma(q,\tau)$ and $\Lambda(\tau)$ are functions of the architecture-dependent expressions provided earlier. Substitution of the appropriate relationships for $\Gamma(q,\tau)$ and $\Lambda(\tau)$ into Eq. 24 provides a complete description of structural evolution during the linear (onset) stage of spinodal decomposition in a reacting polymer blend.

Results and Discussion

Conversion-architecture-phase-stability (CAPS) diagrams

Even a simplified treatment of simultaneous phase separation and chemical reaction requires a multivariate solution, since all of the system characteristics (e.g., initial blend composition, fractions of functionalized chains, reaction rates, and self-diffusion coefficients) significantly influence the behavior of the reacting polymer blend. Conventional phase diagrams are not applicable for mapping relationships between system characteristics and blend phase behavior, since the blend structure varies with time according to the reaction-regulated compatibility and mobility of the constituent chains. To provide a means by which to visualize the process direction (as well as trends in structural evolution), we propose a multifunctional diagram that permits simultaneous mapping of reaction conversion, reaction time, and phase stability (according to the spinodal condition) for specified initial concentrations of available functionalized sites (z_a and z_b). This diagram is referred to as a conversion-architecture-phase-stability (CAPS) diagram. For mapping purposes, Eq. 22a is first rewritten as

$$p_a = \frac{n z_b (1-\phi) f}{z_a \phi (1-f)} p_b. \tag{25}$$

Recall that n denotes the number of reactive sites per B chain: 1 for an AB diblock copolymer, 2 for an ABA triblock copolymer, and $\bar{n}$ for a graft copolymer.

If, for the sake of illustration, z_b is varied while all other parameters remain fixed, Eq. 25 defines a family of straight lines in (p_b, p_a) coordinates. Movement along such a line corresponds to the continuous variation of conversion in blends with varying fractions of functionalized chains. In the same vein, reaction time scales can likewise be mapped onto the diagram using a combination of Eqs. 22a and 22b. To facilitate comparison between these quantities in (p_b, p_a) coordinates, we elect to express the architecture-dependent reaction conversion as the product $\bar{n}z_b$ (the total concentration of reactive sites on B within the blend) and a dimensionless reaction time (τ) as $\alpha t/(a^3 N)$. (For brevity, $\bar{n}$ likewise denotes n in these diagrams unless otherwise indicated.) It is also possible to include spinodal curves on the CAPS diagram. The spinodal curve occurs at the conditions in p_a-p_b space where $\Gamma = 0$ at $q = 0$. Below the resulting curve, the blend undergoes spinodal decomposition and continues to phase-separate, since values of q exist for which $\Gamma(q) < 0$. Above the spinodal curve, $\Gamma(q)$ is everywhere positive, in which case composition fluctuations tend to decrease and blend miscibility is promoted.

Effect of copolymer molecular architecture

Shown in Figure 3 is the CAPS diagram against which all other diagrams presented in subsequent sections are compared. In this diagram, $f = 0.50$ (the chain lengths of the A and B homopolymers comprising the blend are equal), $\phi = 0.50$ (the volumes of the A and B homopolymers are equal), $z_a = 1.00$ (all of the A homopolymers are functionalized and can react), $\chi = 3\chi_c/2$ (the initial quench ends deep within the two-phase region of the phase diagram), and only the diblock ($n = 1$), triblock ($n = 2$), and graft ($\bar{n} = 1.5$) copolymer architectures are considered. Lines passing through the origin and labeled with italicized values correspond to five different values of the product $\bar{n}z_b$ ranging from 0.10 to 1.00. Along the $\bar{n}z_b = 1.00$ line in Figure 3, for example, all of the A chains react with the monofunctionalized B chains (if $n = 1$) so that $p_a = p_b$. Alternatively, if the B chains are bifunctional ($n = 2$), then only half of the B-chain population must be capable of participating in the macromolecular reaction to exhaust the supply of monofunctional A chains, in which case the $p_a = p_b$ line corresponds to $z_b = 0.50$. A similar relationship exists for the graft copolymer with $\bar{n} = 1.5$. Also shown in this figure are five isochrones (curves of constant dimensionless reaction time, τ, which is varied from 0.25 to 3.00), as well as the spinodal lines for the three copolymer architec-

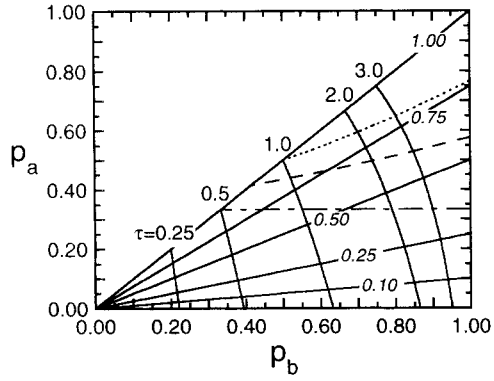

Figure 3. CAPS diagram showing the conversion of A chains (p_a) as a function of the conversion of B chains (p_b) for a reactive polymer blend in which $f = 0.50$, $\phi = 0.50$, $z_a = 1.00$ and $\chi = 3\chi_c/2$.

Straight lines passing through the origin correspond to different values (italicized labels located on the lines) of reactive-site concentrations on the B chains ($\bar{n}z_b$). Isochronal lines (denoting constant reaction times, τ) are provided (and labeled), as are the spinodal lines for blends that form diblock copolymers (dot-dashed line), triblock copolymers (dashed line), and 1.5-arm graft copolymers (dotted line) *in situ* during reactive miscibilization.

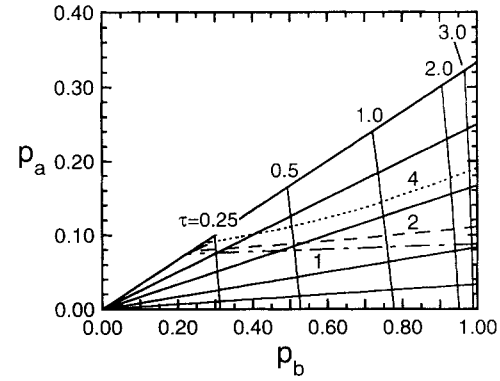

Figure 4. CAPS diagram for a reactive polymer blend in which the mean number of arms per chain of a grafted copolymer ($\bar{n}$) is varied: 1 (dot-dashed line), 2 (dashed line), and 4 (dotted line).

Except for ϕ (= 0.75), all other blend characteristics are the same as those listed in the caption of Figure 3.

tures examined here: diblock (lowest p_a), triblock (intermediate p_a), and graft (highest p_a).

From Figure 3, it can be concluded that, for a given value of $\bar{n}z_b$, reactive miscibilization induced by the *in situ* formation of diblock copolymer molecules occurs more quickly than that promoted by comparable triblock or graft copolymer formation during the early stages of spinodal decomposition. An analogous interpretation of this figure is that, at constant τ, a lower concentration of diblock copolymer molecules is required during reactive blending, relative to that of triblock or graft copolymers, to cross the spinodal line and promote miscibility between the A and B chains. While these trends constitute general features of the CAPS diagrams presented in the following sections, differences arise as the blend characteristics, such as molecular architecture (n vs. $\bar{n}$), chain length (f), blend composition (ϕ), reactive chain fraction (z_a), and quench depth (χ), are varied. We explore the impact of each of these characteristics in the following sections. It should be noted at this juncture that, within the framework of the present mean-field treatment, the dependence of χ on functionality concentration (z_a or z_b) is not considered.

Although the CAPS diagram displayed in Figure 3 clearly demonstrates the effect of molecular architecture on polymer blend miscibilization during early-stage spinodal decomposition, only one graft copolymer (with $\bar{n} = 1.5$) is included in the comparison. In Figure 4, ϕ is increased to 0.75, while the remaining system characteristics (f, z_a, and χ) are the same as those in Figure 3, so that the average number of grafts per copolymer molecule ($\bar{n}$) can be varied from 1 to 4 (while retaining spinodal lines on the CAPS diagram) to ascertain the relative importance of graft number on miscibilization during the onset of reactive blending. It should be borne in mind that a graft copolymer with $\bar{n} = 1$ is not equivalent to a diblock copolymer with $n = 1$, nor does a graft copolymer with $\bar{n} = 2$ correspond to a triblock copolymer with $n = 2$ (see Eqs. 17–19). According to Figure 4, the spinodal lines for the graft copolymers with $\bar{n}$ equal to 1 and 2 are comparable in magnitude (note the difference in the scale of p_a between Figures 3 and 4 due to the difference in ϕ).

When $\bar{n}$ is increased further to 4, Figure 4 reveals that the spinodal line increases markedly (in p_a), especially at large p_b, indicating that blend miscibility is promoted more quickly with graft copolymer molecules possessing few arms. Recall that the present formalism is strictly limited to early-stage spinodal decomposition, in which case the effect of $\bar{n}$ on interfacial structure and ultimate stabilization cannot be suitably addressed. Such a comparison is, however, possible within the limits of self-consistent field theory, as recently demonstrated by Lyatskaya et al. (1995, 1996). Since Figure 4 establishes that an increase in $\bar{n}$ is accompanied by a reduction in initial miscibilization effectiveness, the CAPS diagrams displayed hereafter will retain $\bar{n} = 1.5$. Note that the (italicized) labels on the constant $\bar{n}z_b$ lines in Figure 4 and in subsequent diagrams are omitted to avoid unnecessary confusion due to crowding. The values of $\bar{n}z_b$ associated with these lines are the same as those assigned in Figure 3.

Effect of molecular and blend composition

If the chain lengths of the A and B homopolymers are such that the number fraction of A repeat units in a block copolymer composed of A and B homopolymers (i.e., f) deviates from 0.50 (used to produce Figure 3) by ± 0.25 and all other blend characteristics remain constant, then the resulting CAPS diagrams are observed to change significantly, as seen in Figure 5. The most noticeable features of the diagram in Figure 5a (with $f = 0.25$), relative to Figure 3 (with $f = 0.50$), is the change in p_a scale and the absence of the spinodal line for the graft copolymer with $\bar{n} = 1.5$. Moreover, the isochrone corresponding to $\tau = 3.0$ is not shown due to its close proximity to the edge of the graph at $p_b = 1.00$. At $f = 0.25$, recall that the A chains are one-third the size of the B chains prior to copolymerization. Since ϕ is held constant at 0.50 in Figure 5a, conservation of mass requires an increase in the initial concentration of A chains upon a reduction in f. This

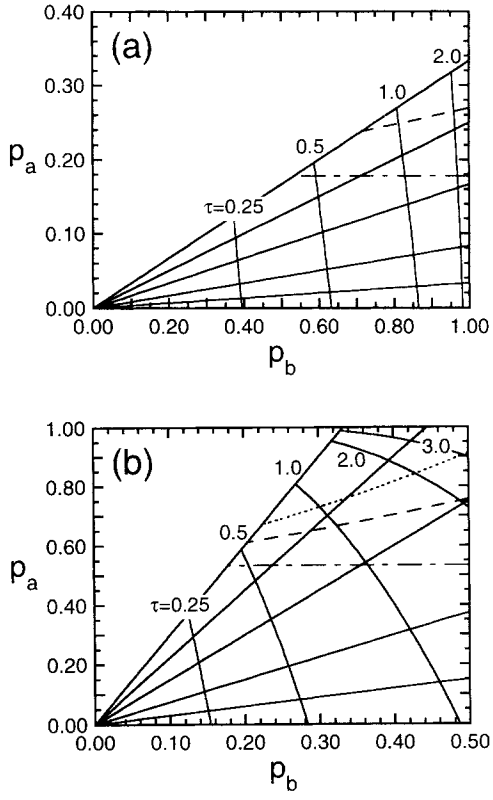

Figure 5. CAPS diagrams for two reactive blends in which the fractional mass of A in the copolymer formed during reactive blending (f) is varied: (a) 0.25 and (b) 0.75.

All other blend characteristics, as well as the symbols used, are the same as those in Figure 3 (in which $f = 0.50$).

increase is evident in Figure 5a, in which the complete conversion of functionalized B chains ($p_b = 1.00$) occurs along the $\bar{n}z_b = 1.00$ line when $p_a < 1.00$. If $f = 0.75$, as in Figure 5b, a spinodal line for the graft copolymer is recovered, and the converse trends of those seen in Figure 5a are observed. That is, the increase in f from 0.50 (Figure 3) to 0.75 (Figure 5b) at constant ϕ is accompanied by a decrease in the number of available A chains, and is responsible for increasing the slopes of the $\bar{n}z_b$ lines so that p_a attains a value of unity when $p_b < 1.00$.

Another blend parameter that must be considered in reactive blending is the blend composition, that is, the fraction of A chains relative to that of B chains. In Figure 3, the volume fraction of A chains (ϕ) is equal to 0.50. In Figure 6a, ϕ is reduced to 0.25, resulting in a shift of the CAPS diagram to lower p_a. Consider once again the $\bar{n}z_b = 1.00$ line for the case in which a diblock copolymer ($n = 1$) is produced during blending. In this case, all of the A molecules react during the copolymerization ($p_a = 1.00$) when only one-third of the B molecules participate in the reaction ($p_b = 0.33$). While Figure 6a ($\phi = 0.25$) resembles Figure 5b ($f = 0.75$) due to the shared reduction in functionalized A chains relative to those available when $\phi = 0.50$ (see Figure 3), the positions of the spinodal lines for the diblock, triblock, and graft copolymer architectures, as well as the positions of the isochrones, differ considerably in the two figures. In Figure 6a, the spinodal lines lie at markedly lower values of p_a than in Figure 5b, indicating that miscibilization is enhanced in blends that are not compositionally symmetric (i.e., one reactive homopolymer is available in excess of the other).

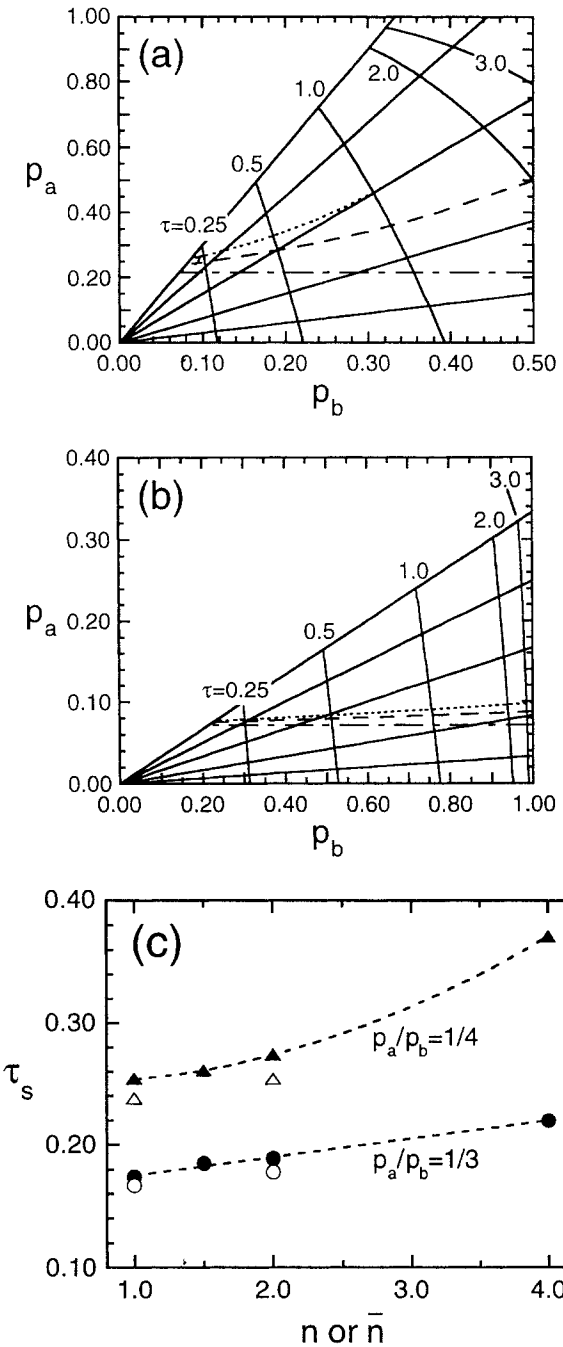

Figure 6. CAPS diagrams for two reactive blends in which the volume fraction of A chains in the blend (ϕ) is varied: (a) 0.25 and (b) 0.75; all other blend characteristics, as well as the symbols used, are the same as those in Figure 3 (in which $\phi = 0.50$).

Shown in (c) is the predicted dimensionless time at the spinodal condition (τ_s) as a function of n (linear copolymers; open symbols) or $\bar{n}$ (graft copolymers; filled symbols) for $\phi = 0.75$ and two cases of constant p_a/p_b: 1/3 (circles) and 1/4 (triangles). The dashed lines serve as guides for the eye.

This trend is likewise evident in Figure 6b, in which ϕ is increased to 0.75. Despite the similarity between Figures 6b ($\phi = 0.75$) and 5a ($f = 0.25$), the positions of both the spinodal and isochronal lines in Figure 6b reveal that the onset of miscibility between A and B is promoted more quickly if the volume fraction of A exceeds that of B (at constant f, as in Figure 6b) rather than if the number of repeat units on the B chains is greater than that on the A chains (at constant ϕ, as in Figure 5a). Just as in Figure 6a, complete copolymerization of reactive B chains ($p_b = 1.00$) into diblock copolymers is seen in Figure 6b to occur upon reaction of only one-third of the A chains ($p_a = 0.33$) along the $\bar{n}z_b = 1.00$ line. Another interesting feature of this figure is that the spinodal lines corresponding to the three molecular architectures discussed in regard to Figure 6a appear nearly indistinguishable, especially if one considers the range of p_a comprising the ordinate of Figure 6b. This feature is likewise evident in Figure 6c, in which the dependence of τ at the spinodal condition (designated τ_s) is presented as a function of n for linear copolymers (diblock and triblock) or $\bar{n}$ for graft copolymers. The parameters employed in these predictions are the same as those in Figures 4 and 6b, and two cases of constant p_a/p_b are examined: 1/3 (along the $\bar{n}z_b = 1.00$ line) and 1/4 (along the $\bar{n}z_b = 0.75$ line). As mentioned earlier, values of τ_s are predicted to be consistently lower for blends reacting to form linear copolymers than corresponding graft copolymers (with $\bar{n} = n$) in both cases, with the difference becoming more exaggerated as p_a/p_b (or, alternatively, $\bar{n}z_b$) is reduced. Figure 6c also reveals that the variation in $\tau_s(\bar{n})$ becomes more pronounced with decreasing p_a/p_b.

The CAPS diagrams presented thus far have examined the effects of varying chain length (copolymer composition, f) and blend composition (volume fraction, ϕ) on p_a and p_b in the limit that all monofunctionalized A chains can participate in the A-B copolymerization during reactive blending of the A and B homopolymers. While the $\bar{n}z_b$ lines in Figures 3–6 permit examination of blend compatibilization in the presence of nonparticipating B chains (i.e., $z_b < 1.00$), no attempt has been made yet to evaluate the effect of nonparticipating A chains (for which $z_a < 1.00$). Figure 3 portrays the case in which all the A chains are capable of coupling with mono/multifunctionalized B chains when $f = \phi = 0.50$. In Figure 7, the concentration of reactive sites on monofunctionalized A chains (z_a) is reduced to 0.75 (Figure 7a) and 0.50 (Figure 7b) under the same conditions of f and ϕ to ascertain the concentration dependence of A chains on early-stage reactive miscibilization.

As z_a is decreased from unity, the isochrones shift to lower values of p_b in a manner such that the condition $p_a = p_b = 1.00$ is met when $z_a = \bar{n}z_b$. Likewise, p_a attains a value of unity along the $\bar{n}z_b = 1.00$ line when $p_b = z_a$, which reflects the complete consumption of reactive A chains. Upon comparing Figures 6a and 7, it is evident that, at constant f (= 0.50), a reduction in the concentration of fully reactive A chains (ϕ) is not equivalent to a reduction in the fraction of reactive A chains (z_a) at constant blend composition. Moreover, as z_a is decreased from unity, the positions of the spinodal lines shift to higher conversions of A (p_a) and longer reaction times (τ), indicating that the onset of miscibility proceeds more slowly if fewer monofunctionalized A chains participate in the copolymerization during reactive blending. The

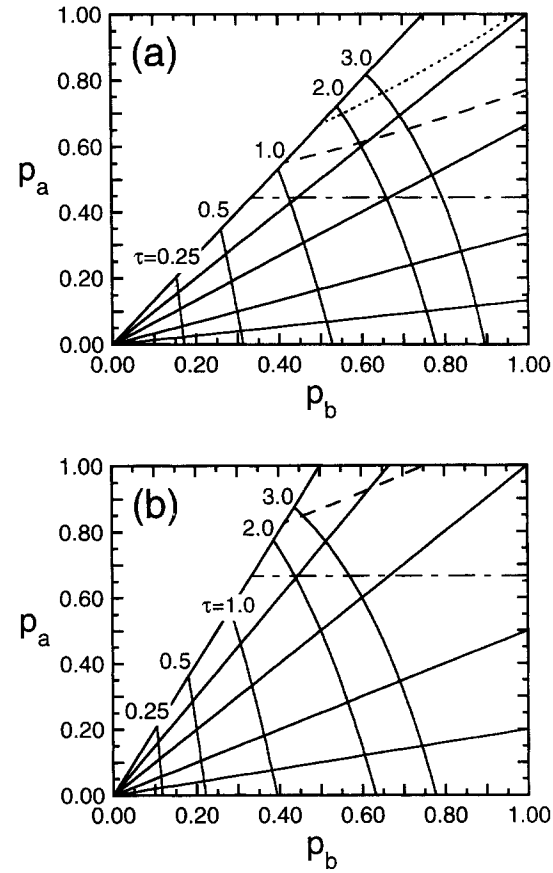

Figure 7. CAPS diagrams for two reactive blends in which the concentration of reactive sites on the A chains in the blend (z_a) is varied: (a) 0.75 and (b) 0.50.

All other blend characteristics, as well as the symbols used, are the same as those in Figure 3 (in which $z_a = 1.00$).

spinodal line corresponding to the 1.5-arm graft copolymer is absent in Figure 7b, since it occurs at longer reaction times than are considered here.

Effects of temperature-induced chemical incompatibility

The last parameter to be examined in this study of early-stage reactive blend miscibilization is the depth of the initial quench from the homogeneous (one-phase) state into the two-phase regime where $\chi > \chi_c$. All of the CAPS diagrams discussed thus far have held χ constant at $3\chi_c/2$. In this section, the effect of varying χ is investigated. Shown in Figure 8 are CAPS diagrams in which the depth of the initial quench (expressed in terms of χ) is increased to $2\chi_c$ (Figure 8a) and $3\chi_c$ (Figure 8b), while all other system parameters are the same as those used to generate Figure 3. As χ is increased in these figures, the $\bar{n}z_b$ and isochronal lines remain invariant, whereas the spinodal lines shift upward to longer reaction times. An increase in χ or, alternatively, a reduction in temperature on a temperature-composition phase diagram is accompanied by an increase in chemical incompatibility between the A and B monomeric units (which serves to promote phase separation).

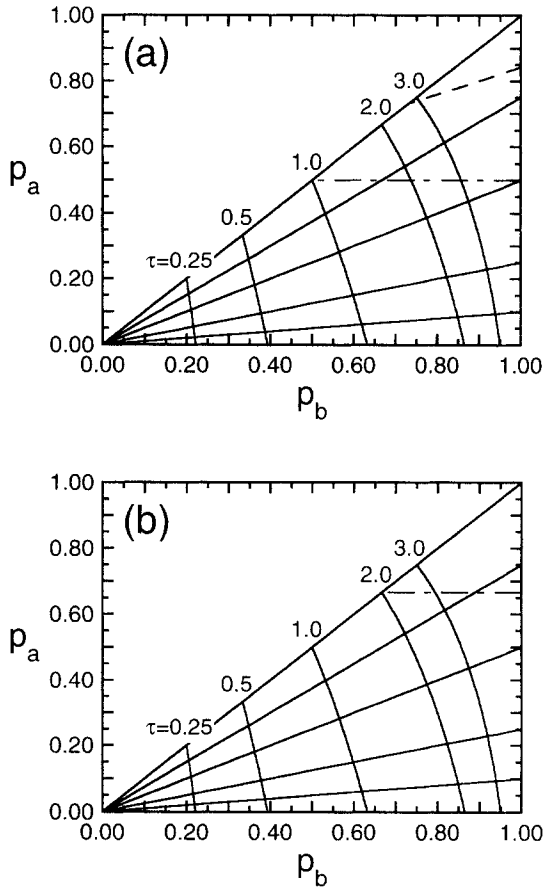

Figure 8. CAPS diagrams for two reactive blends in which the monomeric incompatibility (χ) or, alternatively, the thermal quench depth is varied: (a) $2\chi_c$ and (b) $3\chi_c$.

All other blend characteristics, as well as the symbols used, are the same as those in Figure 3 (in which $\chi = 3\chi_c/2$).

For a given set of blend parameters (f, ϕ, and z_a) and a (p_a, p_b) coordinate corresponding to a predetermined time of reaction (τ), an increase in quench depth results in a reduction in p_a so that the coordinate lies further below the spinodal line on a CAPS diagram. Conversely, as seen in the diagrams displayed in Figures 3, 8a and 8b, the spinodal lines shift upward upon increasing χ. Thus, a deeper quench requires longer reaction times to promote blend miscibility. If we define ϵ as χ/χ_c, then the time τ signaling the onset of miscibility for the case of the diblock copolymer architecture is found to increase linearly with ϵ over the reaction times considered. For the remaining two architectures, the spinodal lines increase beyond the reaction times examined in this work (up to $\tau = 3.0$) as χ is increased, and gradually become inaccessible at relatively short reaction times.

Effect of copolymer architecture on miscibilization dynamics

Through the use of CAPS diagrams, the predictions presented thus far have focused on elucidating the extent to which various factors affect the miscibility of reactive polymer blends. In this section, we address the dynamics of structural development during reactive miscibilization. Displayed in Figure 9 is the time evolution of the structure factor, $S(q,t)$, evaluated from Eq. 24 relative to the structure factor at initial time, $S(q,0)$ at $q = q_{max}$, the wave vector at which composition fluctuations grow most quickly during the spinodal decomposition of a nonreacting blend at the conditions listed in Figure 6a (with $z_b = 0.5$ and $N = 1000$). In Figure 9, this structure factor ratio is shown as a function of dimensionless spinodal decomposition time (t_{SD}) (Binder, 1994), where $t_{SD} = k\tau$ ($k = 3.61$ in Figure 9a and $k = 0.361$ in Figure 9b), for two values of $\alpha/(Da)$: 1.0 (Figure 9a) and 0.1 (Figure 9b). Since the diffusion-controlled regime occurs at $\alpha/(DaN^{1/2}) \sim 1$ (Frederickson and Milner, 1996), these values of $\alpha/(Da)$ ensure that the blends considered here reside within the kinetically controlled regime. The predictions in Figure 9 are based on a homogeneous blend initially at $\chi_0 = 0$ and then quenched to $\chi = 3\chi_c/2$. While $S(q_{max},t_{SD})/S(q_{max},0)$ de-

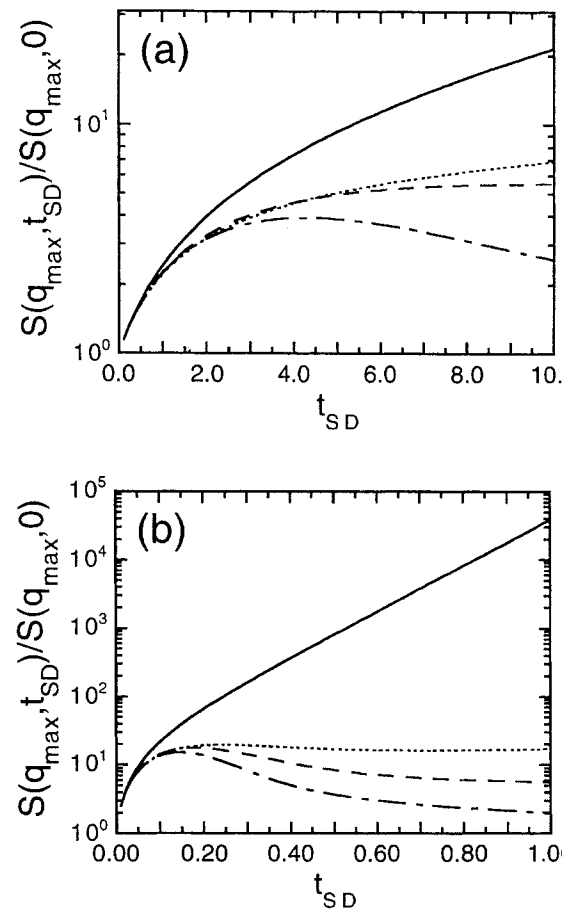

Figure 9. Evolution of the normalized structure factor $S(q_{max},t_{SD})/S(q_{max},0)$, where q_{max} denotes the wave vector at which composition fluctuations grow most quickly during spinodal decomposition, presented as a function of t_{SD} ($\propto \tau$) for two values of $\alpha/(Da)$: (a) 1.0 and (b) 0.1.

Shown here are predictions for the nonreacting blend (solid line) and analogous blends composed of reactive chains that generate diblock, triblock, and 1.5-arm graft copolymers (dot-dashed, dashed, and dotted lines, respectively) at the conditions listed in Figure 6a (with $z_b = 0.5$ and $N = 1000$).

pends on the choice of χ_0, the predictions in Figure 9 provide qualitatively general trends. Since the slope of each curve in Figure 9 is a measure of the rate at which fluctuations change in the phase-separating blend, curves with a positive slope everywhere indicate that composition fluctuations grow with time, and spinodal decomposition proceeds, as is evident for the nonreacting blends.

In Figure 9a, production of 1.5-arm graft copolymers during phase separation results in a reduction in the rate of spinodal decomposition over the range of t_{SD} examined. Since the slope of the corresponding curve remains positive, phase separation continues during the course of reaction (in accord with the predictions in Figure 6a), but is significantly slowed. In the case of the reaction yielding a triblock copolymer, $S(q_{max}, t_{SD})/S(q_{max}, 0)$ becomes independent of time, revealing that the growth of fluctuations in the blend is halted due to the presence of copolymer molecules. Over the same t_{SD} interval, the blend of monofunctional A and B chains (which yield diblock copolymer molecules upon reaction) exhibits a maximum in $S(q_{max}, t_{SD})/S(q_{max}, 0)$. As with the triblock copolymer, this maximum identifies the time at which composition fluctuations stop growing. At longer times, where the slope of the $S(q_{max}, t_{SD})/S(q_{max}, 0)$ vs. t_{SD} curve becomes negative, fluctuations decay and the blend becomes decreasingly less structured. Similar behavior is seen in Figure 9b, wherein $\alpha/(Da) = 0.1$ (this blend lies further inside the kinetically controlled regime than the one employed in Figure 9a). In Figure 9b, the $S(q_{max}, t_{SD})/S(q_{max}, 0)$ vs. t_{SD} curves for all three reactive blends exhibit a maximum and possess slopes approaching zero in the vicinity of $t_{SD} = 1.0$. This latter observation indicates that these reactive blends have reached late-stage miscibilization, in which structural variations are negligibly small and a final blend structure is achieved.

In general, it must be recognized that the production of block copolymers from two reactive homopolymers undergoing spinodal decomposition constitutes an effective means by which to reduce the rate at which phase separation occurs in the blend, and therefore promotes blend miscibilization. According to the predictions displayed in Figure 9b, the magnitude of this effect can be substantial: $S(q_{max}, t_{SD})/S(q_{max}, 0)$ lies between 2 and 20 for all three copolymer architectures at $t_{SD} = 1.0$, whereas the corresponding value for the nonreacting blend is $\approx 40{,}000$. Thus, beyond an early induction period, reactive blends are (in some cases, considerably) less structured at any time during spinodal decomposition than the nonreacting parent blend. As pointed out in the previous section and confirmed by the predictions in Figure 9, production of diblock copolymer molecules from monofunctional A and B chains appears to promote the most expedient miscibilization (measured in terms of both the onset of fluctuation decay and the ultimate level of blend structure) of the three copolymer architectures examined here.

Conclusions

Reactive processing constitutes a commercially important method by which to compatibilize immiscible homopolymers (i.e., control the size scale of phase-separated domains) through the *in situ* production of block/graft copolymers. In this work, we consider an extension of this approach in which the *miscibility* of a polymer blend undergoing phase separation by spinodal decomposition in the biphasic region of the phase diagram is likewise controlled through reactive chain coupling. A theoretical framework based on the random phase approximation (de Gennes, 1979) has been used to examine the principal factors regulating the reactive miscibilization of two macromolecules exhibiting UCST behavior during early-stage spinodal decomposition, which is kinetically governed and can therefore be described by a mean-field treatment. By allowing one homopolymer to be monofunctional and the other to be either monofunctional (to form $\bar{n}$-arm graft copolymers), bifunctional (to form triblock copolymers), or multifunctional (to form $\bar{n}$-arm graft copolymers), we have analyzed the effect of copolymer architecture on blend miscibility at the onset of phase separation. According to the results presented here, diblock copolymer formation during reactive blending promotes miscibility at the shortest time scales. Other blend parameters probed here include homopolymer chain length, bulk blend composition, functionalized homopolymer fractions, and the thermal quench depth (into the biphasic region of the phase diagram).

While the theoretical formalism proposed here is incapable of addressing the factors governing structure coarsening during the late-stage spinodal decomposition of reactive blends (Frederickson and Milner, 1996), it provides insight into the relative importance of blend characteristics during early-stage miscibilization through the use of CAPS diagrams. These diagrams constitute a multifunctional representation of reactant conversion/blend miscibility in terms of (1) homopolymer reactive functionality concentration; (2) blend reaction time; and (3) architecture-dependent spinodal lines. Factors responsible for increases in the miscibilization time of phase-separating polymer blends include incomplete homopolymer conversion and an increase in the depth of the initial quench into the two-phase regime (expressed in terms of χ relative to χ_c). The time evolution of the structure factor reveals that spinodal decomposition can be slowed dramatically in immiscible blends of reactive homopolymers. In agreement with results obtained from the CAPS diagrams, dynamic miscibilization is most expediently achieved through the use of monofunctional chains that react to form diblock copolymer molecules.

Acknowledgments

This work was supported by a COBASE grant from the National Research Council. We are grateful to two of the reviewers for valuable comments and suggestions.

Literature Cited

Balsara, N. P., "Thermodynamics of Polymer Blends," *Physical Properties of Polymers Handbook*, Chap. 19, J. E. Mark, ed., AIP Press, New York (1996).

Bates, F. S., "Polymer-Polymer Phase Behavior," *Science*, **251**, 898 (1991).

Binder, K., "Phase Transitions in Polymer Blends and Block Copolymer Melts: Some Recent Developments," *Adv. Polym. Sci.*, **112**, 181 (1994).

Bonner, J. G., and P. S. Hope, "Compatibilisation and Reactive Blending," *Polymer Blends and Alloys*, Chap. 3, M. J. Folkes and P. S. Hope, eds., Chapman & Hall, London (1993).

Cigana, P., B. D. Favis, and R. Jérôme, "Diblock Copolymers as Emulsifying Agents in Polymer Blends: Influence of Molecular Weight, Architecture, and Chemical Composition," *J. Poly. Sci. B: Poly. Phys.*, **34**, 1691 (1996).

Creton, C., E. J. Kramer, and G. Hadziioannou, "Critical Molecular Weight for Block Copolymer Reinforcement of Interfaces in a 2-Phase Polymer Blend," *Macromol.*, **24**, 1846 (1991).
Dai, K. H., J. Washiyama, and E. J. Kramer, "Segregation Study of a BAB Triblock Copolymer at the A/B Homopolymer Interface," *Macromol.*, **27**, 4544 (1994).
Dai, C., K. D. Jandt, D. R. Iyengar, N. L. Slack, K. H. Dai, W. B. Davidson, E. J. Kramer, and C. Y. Hui, "Strengthening Polymer Interfaces with Triblock Copolymers," *Macromol.*, **30**, 549 (1997).
Datta, S., and D. J. Lohse, *Polymeric Compatibilizers: Uses and Benefits in Polymer Blends*, Hanser, Munich (1996).
de Gennes, P.-G., "Reptation of a Polymer Chain in the Presence of Fixed Obstacles," *J. Chem. Phys.*, **55**, 572 (1971).
de Gennes, P.-G., *Scaling Concepts in Polymer Physics*, Chaps 4 and 9, Cornell Univ. Press, Ithaca, NY (1979).
de Gennes, P.-G., "Kinetics of Diffusion-Controlled Processes in Dense Polymer Systems: I. Non-Entangled Regimes," *J. Chem. Phys.*, **76**, 3316 (1982a).
de Gennes, P.-G., "Kinetics of Diffusion-Controlled Processes in Dense Polymer Systems, II. Effects of Entanglements," *J. Chem. Phys.*, **76**, 3322 (1982b).
Feng, Y., R. A. Weiss, and C. C. Han, "Compatibilization of Polymer Blends by Complexation: 3. Structure Pinning during Phase Separation of Ionomer/Polyamide Blends," *Macromol.*, **29**, 3925 (1996).
Fleischer, C. A., A. R. Morales, and J. T. Koberstein, "Interfacial Modification Through End Group Complexation in Polymer Blends," *Macromol.*, **27**, 379 (1994).
Fredrickson, G. H., and L. Leibler, "Theory of Diffusion-Controlled Reactions in Polymers Under Flow," *Macromol.*, **29**, 2674 (1996).
Fredrickson, G. H., and S. T. Milner, "Time-Dependent Reactive Coupling at Polymer-Polymer Interfaces," *Macromol.*, **29**, 7386 (1996).
Guégan, P., C. W. Macosko, T. Ishizone, A. Hirao, and S. Nakahama, "Kinetics of Chain Coupling at Melt Interfaces," *Macromol.*, **27**, 4993 (1994).
Hashimoto, T., and T. Izumitani, "Effect of a Block Copolymer on the Kinetics of Spinodal Decomposition of Polymer Blends: 1. Nonuniversality in Scaled Characteristic Quantities versus Reduced Time," *Macromol.*, **26**, 3631 (1993).
He, M. J., Y. M. Liu, F. Yi, J. Ming, and C. C. Han, "Spinodal Decomposition in a Hydrogen-Bonded Polymer Blend," *Macromol.*, **24**, 464 (1991).
Kawasaki, K., and K. Sekimoto, "Concentration Dynamics in Polymer Blends and Block Copolymer Melts," *Macromol.*, **22**, 3063 (1989).
Kramer, E. J., P. F. Green, and C. Palmstrom, "Interdiffusion and Marker Movements in Concentrated Polymer-Polymer Diffusion Couples," *Polymer*, **25**, 473 (1984).
Kumpf, R. J., J. S. Wiggins, and H. Pielartzik, "Reactive Processing of Engineering Thermoplastics," *Trends Poly. Sci.*, **3**, 132 (1995).
Lyatskaya, Y., D. Gersappe, and A. C. Balazs, "Effect of Copolymer Architecture on the Efficiency of Compatibilizers," *Macromol.*, **28**, 6278 (1995).
Lyatskaya, Y., D. Gersappe, N. A. Gross, and A. C. Balazs, "Designing Compatibilizers to Reduce Interfacial Tension in Polymer Blends," *J. Phys. Chem.*, **100**, 1449 (1996).
Macosko, C. W., P. Guégan, A. K. Khandpur, A. Nakayama, P. Marechal, and T. Inoue, "Compatibilizers for Melt Blending: Premade Block Copolymers," *Macromol.*, **29**, 5590 (1996).
Milner, S. T., "How do Copolymer Compatibilizers Really Work?" *Mater. Res. Soc. Bull.*, **22**, 38 (1997).
Noolandi, J., and K. M. Hong, "Interfacial Properties of Immiscible Homopolymer Blends in the Presence of Block Copolymers," *Macromol.*, **15**, 482 (1982).
O'Shaughnessy, B., "Effect of Concentration on Reaction Kinetics in Polymer-Solutions," *Macromol.*, **27**, 3875 (1994).
O'Shaughnessy, B., and U. Sawhney, "Reaction Kinetics at Polymer-Polymer Interfaces," *Macromol.*, **29**, 7230 (1996).
Piirma, I., *Polymeric Surfactants*, Chap. 8, Dekker, New York (1992).
Platé, N. A., A. D. Litmanovich, and O. V. Noah, *Macromolecular Reactions: Peculiarities, Theory and Experimental Approaches*, Chaps. 6 and 7, Wiley, New York (1995).
Scott, C., and C. Macosko, "Model Experiments for the Interfacial Reaction Between Polymers during Reactive Polymer Blending," *J. Poly. Sci. B: Poly. Phys.*, **32**, 205 (1994).
Scott, C. E., and C. W. Macosko, "Processing and Morphology of Polystyrene/Ethylene-Propylene Rubber Reactive and Nonreactive Blends," *Poly. Eng. Sci.*, **35**, 1938 (1995).
Sillescu, H., "Relation of Interdiffusion and Tracer Diffusion in Polymer Blends," *Makromol. Chem., Rapid Commun.*, **8**, 393 (1987).
Sundararaj, U., and C. W. Macosko, "Drop Breakup and Coalescence in Polymer Blends: The Effects of Concentration and Compatibilization," *Macromol.*, **28**, 2647 (1995).
Tanaka, H., T. Suzuki, T. Hayashi, and T. Nishi, "New Type of Pattern Formation in Polymer Mixtures Caused by Competition Between Phase Separation and Chemical Reaction," *Macromol.*, **25**, 4453 (1992).
Wool, R. P., *Polymer Interfaces: Structure and Strength*, Chap. 2, Hanser, Munich (1995).
Yashin, V. V., Ya. V. Kurryavtsev, E. Govorun, and A. Litmanovich, "Macromolecular Reaction and Interdiffusion in a Compatible Polymer Blend," *Macromol. Theory Simul.*, **6**, 247 (1997).

Manuscript received Apr. 7, 1997, and revision received Sept. 29, 1997.